



Article

Structural Features Promoting Photocatalytic Degradation of Contaminants of Emerging Concern: Insights into Degradation Mechanism Employing QSA/PR Modeling

 Antonija Tomic¹, Marin Kovacic¹ , Hrvoje Kusic^{1,2,*}, Panaghiotis Karamanis³, Bakhtiyor Rasulev⁴  and Ana Loncaric Bozic¹
¹ Faculty of Chemical Engineering and Technology, University of Zagreb, Marulicev Trg 19, 10000 Zagreb, Croatia

² Department for Packaging, Recycling and Environmental Protection, University North, Trg dr. Žarka Dolinara 1, 48000 Koprivnica, Croatia

³ E2S UPPA, CNRS, IPREM, Université de Pau et des Pays de l'Adour, Hélioparc Pau Pyrénées, 2 Rue de President Angot, 64053 Pau, France

⁴ Department of Coatings and Polymeric Materials, North Dakota State University, Fargo, ND 58102, USA

* Correspondence: hkusic@fkit.hr; Tel.: +385-1-4597-160

Abstract: Although heterogeneous photocatalysis has shown promising results in degradation of contaminants of emerging concern (CECs), the mechanistic implications related to structural diversity of chemicals, affecting oxidative (by HO•) or reductive (by O₂•⁻) degradation pathways are still scarce. In this study, the degradation extents and rates of selected organics in the absence and presence of common scavengers for reactive oxygen species (ROS) generated during photocatalytic treatment were determined. The obtained values were then brought into correlation as *K* coefficients ($M_{HO\bullet}/M_{O_2\bullet^-}$), denoting the ratio of organics degraded by two occurring mechanisms: oxidation and reduction via HO• and O₂•⁻. The compounds possessing $K \gg 1$ favor oxidative degradation over HO•, and vice versa for reductive degradation (i.e., if $K \ll 1$ compounds undergo reductive reactions driven by O₂•⁻). Such empirical values were brought into correlation with structural features of CECs, represented by molecular descriptors, employing a quantitative structure activity/property relationship (QSA/PR) modeling. The functional stability and predictive power of the resulting QSA/PR model was confirmed by internal and external cross-validation. The most influential descriptors were found to be the size of the molecule and presence/absence of particular molecular fragments such as C – O and C – Cl bonds; the latter favors HO•-driven reaction, while the former the reductive pathway. The developed QSA/PR models can be considered robust predictive tools for evaluating distribution between degradation mechanisms occurring in photocatalytic treatment.

Keywords: contaminants of emerging concern; TiO₂ photocatalysis; degradation; structural influence; QSA/PR modeling



Citation: Tomic, A.; Kovacic, M.; Kusic, H.; Karamanis, P.; Rasulev, B.; Loncaric Bozic, A. Structural Features Promoting Photocatalytic Degradation of Contaminants of Emerging Concern: Insights into Degradation Mechanism Employing QSA/PR Modeling. *Molecules* **2023**, *28*, 2443. <https://doi.org/10.3390/molecules28062443>

Academic Editor: Miaomiao Ye

Received: 17 February 2023

Revised: 1 March 2023

Accepted: 3 March 2023

Published: 7 March 2023

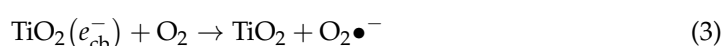
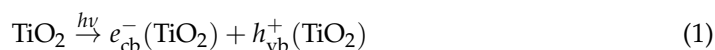


Copyright: © 2023 by the authors. Licensee MDPI, Basel, Switzerland. This article is an open access article distributed under the terms and conditions of the Creative Commons Attribution (CC BY) license (<https://creativecommons.org/licenses/by/4.0/>).

1. Introduction

Contaminants of emerging concern (CECs), such as pharmaceuticals, personal care products, industrial chemicals, per- and polyfluoroalkyl substances (PFASs), and pesticides, have raised strong concerns due to their potential bioaccumulative and toxic characteristics [1–3]. Hundreds of thousands of tons of CECs are dispensed and consumed annually worldwide and are continuously discharged into the environment through wastewater treatment plant (WWTP) effluents [4]. Thus, CECs have been detected in various environmental matrices, causing adverse effects such as increased resistance of microorganisms to antibiotics, acute or chronic toxicity, uncertainties related to transformation products and metabolites, and endocrine-disrupting effects [1,5]. Accordingly, the upgrade of WWTPs by advanced treatment technologies as a tertiary step is required to ensure the elimination

of health risks posed by CECs in water [5,6]. Advanced oxidation/reduction processes (AO/RPs), which generate highly reactive oxygen species (ROS) (e.g., hydroxyl radicals, HO•; superoxide radicals, O₂•⁻; perhydroxyl radicals, HO₂•; hydrogen peroxide, H₂O₂; etc.), either in situ or via the activation of added oxidants/reductants/catalysts, have been shown to be effective for elimination of CECs [7–9]. Among AO/RPs, heterogeneous photocatalysis, based on well-known reactions (Equations (1)–(3)) initiated by the activation of semiconducting material illuminated by sufficient energy, as follows,



have shown promising effectiveness and suitability for the removal of persistent contaminants [10–12]. Titanium dioxide (TiO₂) appears to be the most extensively studied and used photocatalyst, with still the highest potential for use in the commercial application of photocatalytic treatments [13,14] due to properties such as high stability, cost-effective and favorable performance [10,15]. The effectiveness of photocatalytic treatment, besides key process parameters such as pH and TiO₂ loading, strongly depends on the structure of organics present. Namely, process parameters such as pH would dictate (i) positive/negative charge of TiO₂ surface; (ii) present organics in deprotonated or protonated form of undergoing adsorption/degradation; and (iii) susceptibility of compounds to being adsorbed at the photocatalyst surface and be directly degraded there by photogenerated charges (TiO₂(h_{vb}⁺) and TiO₂(e_{cb}⁻)). TiO₂ loading dictates the amount of generated ROS, but also the photo-shielding effect within the reactor space when present in excess [10,15]. On the other hand, the structure of organics would dictate whether degradation undergo preferably oxidation or reduction mechanism. These mechanisms occur simultaneously, but not to the same extent, and consequently, pathways and formed transformation products of organics would differ, affecting the overall quality of treated water in terms of toxicity and biodegradability [16–18]. Hence, Chen et al. [19] investigated the kinetics of photocatalytic degradation of aliphatic carboxylic acids by UV/TiO₂; the results revealed that the degradation mechanism and its efficiency depend on structural features of studied aliphatics, particularly the number of carboxylic groups—more -COOH groups would yield higher degradation rate. However, they did not provide deeper investigation of occurring mechanisms. Furthermore, Yin et al. [20] investigated the degradation of eight aliphatic halogenated contaminants in synthetic drinking water by UVA/TiO₂ and UVA/Cu-TiO₂ processes, and established relationships between degradation rate constants and structural characteristics of studied organics by quantitative structure activity/property relationship (QSA/PR) models. Namely, the degradation of contaminants possessing more polar electron withdrawing moieties and higher degrees of chlorination is strongly promoted in UV-A/TiO₂. Additionally, Huang et al. [21] studied photocatalytic degradation of sulfonamides from the structure-dependent point of view; the findings revealed that degradation rates are strongly related E_{HOMO} values, presumably due to the importance of such moiety in HO• attack [22]. It should be noted that these studies were performed on a limited number (≤10 in each study) of organics with rather high similarities within their structures (e.g., aliphatics in the first two studies, sulfonamides in the third study).

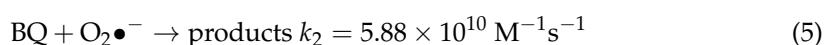
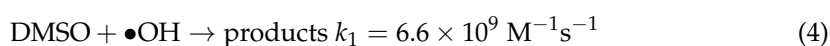
There are numerous studies investigating structure-dependent reactivity of organics with HO• derived within various environmental systems/applications [22–27]. However, studies directed toward O₂•⁻ reactivity are rather scarce, particularly related to water treatment systems [20,27]. To the best of our knowledge, studies comprehending the simultaneous involvement of main oxidative and reductive species, HO• and O₂•⁻, respectively, in photocatalytic systems from the structure–activity aspect have not been performed. Hence, in this study, we investigated the influence of structural features of CECs on their photocatalytic degradation to get insight into the mechanistic aspects fa-

cilitating simultaneous indirect oxidation and reduction (i.e., in the bulk). To that end, we have employed QSA/PR modeling to establish the susceptibility of organics based on their molecular structures for oxidative (via HO•) and reductive (O₂•⁻) degradation by UVA/TiO₂ process.

2. Results and Discussion

2.1. Photocatalytic Degradation of Selected Organics

The photocatalytic degradation of organics can occur via one of two mechanisms: (i) direct, occurring at the photocatalyst surface by photogenerated holes (*h*⁺) and electrons (*e*⁻); and (ii) indirect, occurring in the bulk by ROS, primarily HO• and O₂•⁻, generated as products of reactions of HO⁻ (as water dissociates) and O₂ (dissolved) with photogenerated *h*⁺ and *e*⁻, respectively (Equations (2) and (3)) [9,10,15]. In this study, we focus only on the indirect degradation by ROS, and in that purpose, experiments with dimethyl sulfoxide (DMSO) and benzoquinone (BQ) as effective scavenging agents for HO• and O₂•⁻, respectively (Equations (4) and (5)), were performed [16,28].



The scavenging agents used are effective due to the fact that react with targeted ROS at considerably high rates [29,30]. Taking into account their having a concentration 200 times higher than that of the studied organics in reaction mixture (10 mM >> 0.05 mM), ROS reactions with organics instead of scavenging agents are practically disabled. Prior experiments with scavenging agents, several blanks were performed to elucidate susceptibility of studied organics to be removed/degraded due to hydrolysis and photolysis under the UVA irradiation applied. It was established that none of the studied organics undergo hydrolysis to a significant degree; the removed portions were <0.1% within studied time course of 1 h, which covers both periods of treatment: initial dark and under UVA irradiation (results not shown). Similarly, no significant changes were recorded in photolysis experiments under UVA irradiation in the absence of TiO₂ P25 photocatalyst over a 1 h course; portions of <0.2% were removed in all cases (results not shown). Hence, it can be established that bulk degradation occurs exclusively via ROS reactions. Besides these blank tests, we also tested the tendency of studied organics to be adsorbed onto TiO₂ P25 surface, and as such to be removed from the reaction solution via the sorption process. A detailed investigation of the adsorption capacity of TiO₂ P25 toward the studied organics, accompanied by response surface and QSA/PR modeling, was conducted in previous research [31], while we focus here only on the adsorption at applied photocatalytic process conditions (pH 7 and TiO₂ loading of 0.8 gL⁻¹). Most of the studied organics, as many as 17 compounds, showed very low removal (between 0 and 2%) by adsorption. Furthermore, low removal by adsorption (between 3 to 5%) was recorded for five compounds (EE2, DSL, DCF, DPH and SalAc), while higher removal values are recorded for the following organics: AMX and VZD (11%), ETD (15%), OMP (17%), TB (21%), OXY (27%) and BPA and CIP (31%) (Table S1, Supplementary Materials). In order to investigate the potential of these eight compounds for the direct degradation occurring at the catalyst surface by photogenerated *h*⁺ and *e*⁻, additional experiments with the addition of both ROS scavenging agents simultaneously (DMSO and BQ) were performed in order to suppress bulk reactions. After that, we have performed desorption tests to determine remained concentration adsorbed at the catalyst surface. In all cases, desorbed concentration corresponded to the values established as adsorbed at the catalyst surface during the initial dark period (within the mentioned experimental error). Accordingly, it can be concluded that direct oxidation/reduction of studied organics is not favorable in the studied time course, and that the majority of degradation occurs in the bulk. Hence, we were able to compare the degradation extents in tests with scavenging agents DMSO and BQ to those without, deducting the adsorbed amount from the overall concentration of targeted compound. Accordingly, we established the portion in

overall degradation extent of each organic which pertained to photocatalytic degradation mediated by $\text{HO}\bullet$ and $\text{O}_2\bullet^-$. The results for all 30 organics studied are presented in Figures 1 and 2, and summarized in Table S1.

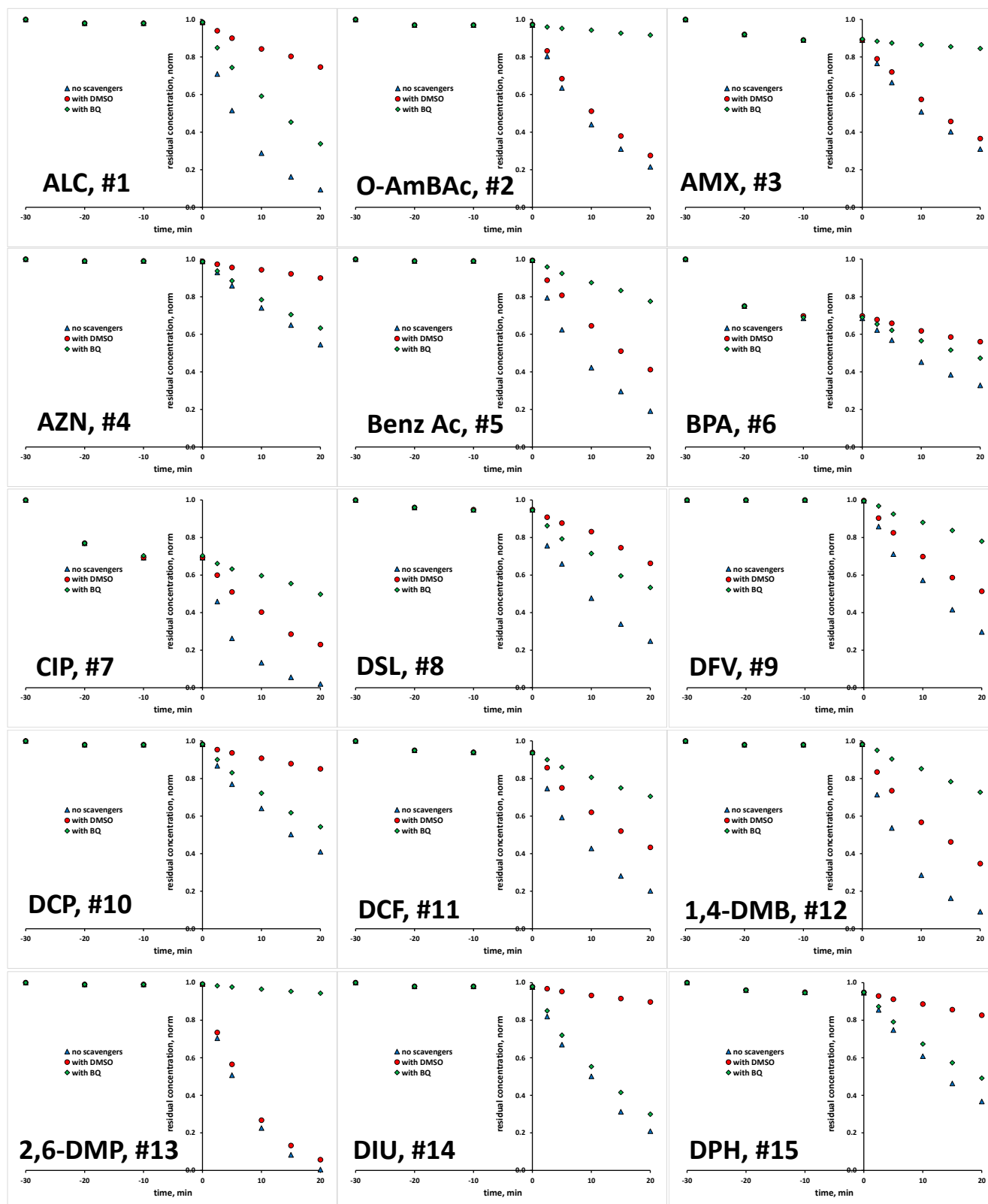


Figure 1. Degradation kinetics of studied organics (#1–15, Table 1) without and with the presence of scavengers for $\text{HO}\bullet$ and $\text{O}_2\bullet^-$.

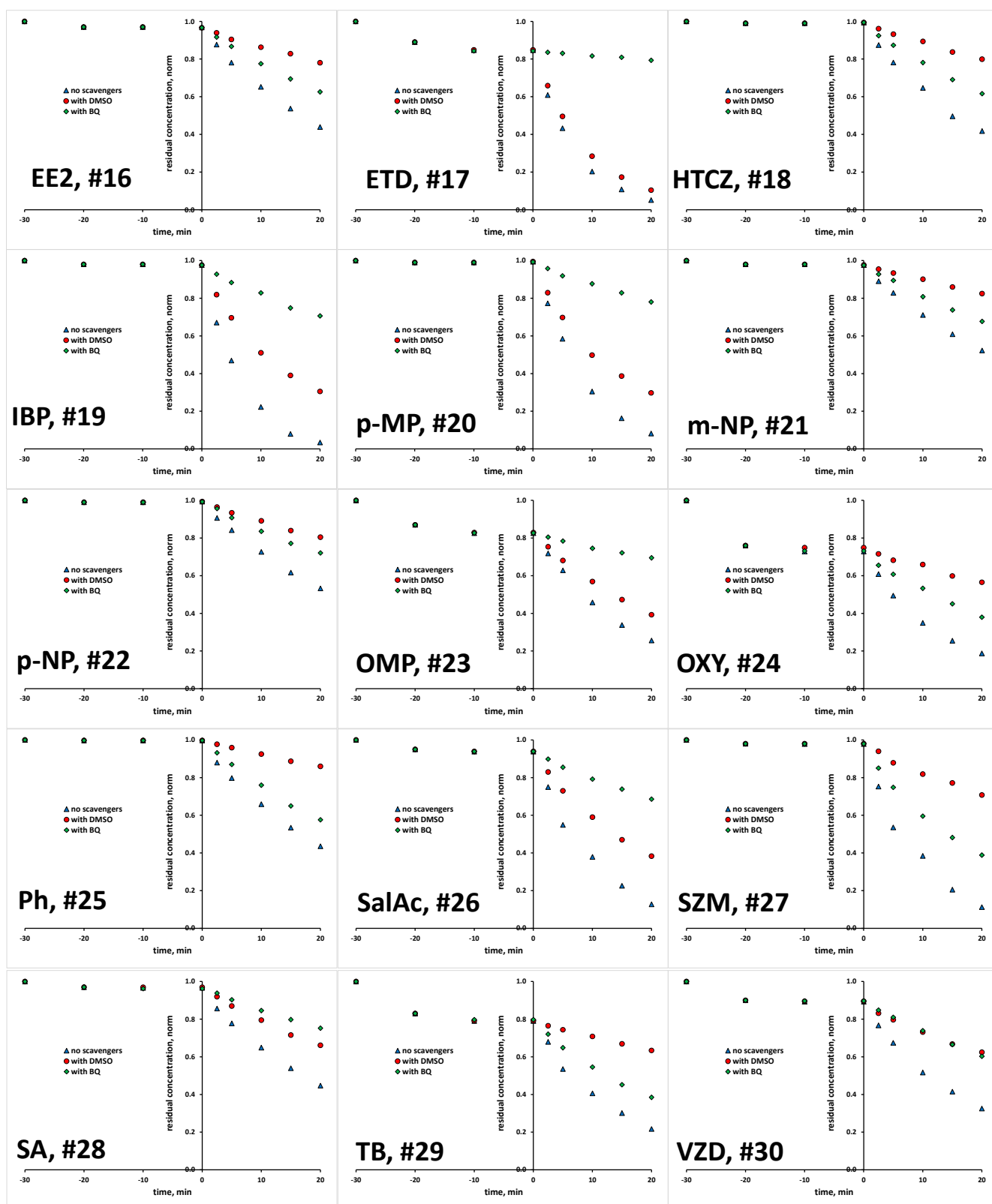


Figure 2. Degradation kinetics of studied organics (#16–30, Table 1) without and with the presence of scavengers for $\text{HO}\bullet$ and $\text{O}_2\bullet^-$.

Table 1. List of 30 selected organics used in a study, along with original and transformed values of *K* coefficient, with included splitting into training and *test* set for QSA/PR modeling.

#	Compound	Abbreviation	CAS	Molecular Formula	<i>K</i>	$\frac{1}{\sqrt{(K+1)}}$
1	Alachlor	ALC	15972-60-8	C ₁₄ H ₂₀ ClNO ₂	2.722	0.518
2	o-Aminobenzoic acid	o-aminoBenzAc	118-92-3	C ₇ H ₇ NO ₂	0.079	0.963
3	Amoxicillin	AMX	26787-78-0	C₁₆H₁₉N₃O₅S	0.095	0.956
4	Atrazine	AZN	1912-24-9	C ₈ H ₁₄ ClN ₅	4.017	0.446
5	Benzoic acid	BenzAc	65-85-0	C ₆ H ₅ COOH	0.374	0.853
6	Bisphenol A	BPA	80-05-7	C ₁₅ H ₁₆ O ₂	1.580	0.623
7	Ciprofloxacin	CIP	85721-33-1	C₁₇H₁₈FN₃O₃	0.852	0.735
8	Desloratadine	DSL	100643-71-8	C ₁₉ H ₁₉ ClN ₂	1.442	0.640
9	Desvenlafaxine	DVF	93413-62-8	C ₁₆ H ₂₅ NO ₂	0.445	0.832
10	2,4-Dichlorophenol	DCP	120-83-2	C ₆ H ₄ Cl ₂ O	3.358	0.479
11	Diclofenac	DCF	15307-79-6	C ₁₄ H ₁₀ Cl ₂ NNaO ₂	0.457	0.829
12	1,4-Dimethoxybenzene	1,4-DMB	150-78-7	C₆H₄(OCH₃)₂	0.400	0.845
13	2,6-Dimethoxyphenol	2,6-DMP	91-10-1	(CH ₃ O) ₂ C ₆ H ₃ OH	0.053	0.974
14	Diuron	DIU	330-54-1	C ₉ H ₁₀ Cl ₂ N ₂ O	8.358	0.327
15	Donepezil HCl	DPH	120011-70-3	C ₂₄ H ₃₀ ClNO ₃	1.404	0.645
16	17α-Ethinylestradiol	EE2	57-63-6	C ₂₀ H ₂₄ O ₂	1.833	0.594
17	Etodolac	ETD	41340-25-4	C ₁₇ H ₂₁ NO ₃	0.067	0.968
18	Hydrochlorothiazide	HCTZ	58-93-5	C ₇ H ₈ ClN ₃ O ₄ S ₂	1.940	0.583
19	Ibuprofene	IBP	15687-27-1	C ₁₃ H ₁₈ O ₂	0.402	0.844
20	p-Methoxyphenol	p-MP	150-76-5	CH₃OC₆H₄OH	0.305	0.875
21	m-Nitrophenol	m-NP	554-84-7	O ₂ NC ₆ H ₄ OH	1.965	0.581
22	p-Nitrophenol	p-NP	100-02-7	O ₂ NC ₆ H ₄ OH	1.437	0.641
23	Omeprazole HCl	OMP	73590-58-6	C ₁₇ H ₂₀ ClN ₃ O ₃ S	0.302	0.876
24	Oxytetracycline	OXY	79-57-2	C ₂₂ H ₂₄ N ₂ O ₉	1.916	0.586
25	Phenol	Ph	108-95-2	C ₆ H ₅ OH	3.069	0.496
26	Salicylic acid	SalAc	69-72-7	C ₇ H ₆ O ₃	0.455	0.829
27	Simazine	SZM	122-34-9	C₇H₁₂ClN₅	2.171	0.562
28	Sulfanilic acid	SA	121-57-3	C ₆ H ₇ NO ₃ S	0.682	0.771
29	Tobramycin	TB	32986-56-4	C ₁₈ H ₃₇ N ₅ O ₉	2.614	0.526
30	Vilazodone HCl	VZD	163521-08-2	C ₂₆ H ₂₇ N ₅ O ₂	1.084	0.693

These relative values were then brought into correlation by creating the *K* coefficient, which denotes ratio of organics degraded by HO• (*M*_{HO•}) vs. that driven by O₂•⁻ (*M*_{O₂•⁻}) (Equation (6)).

$$K = \frac{M_{HO\bullet}}{M_{O_2\bullet^-}} \quad (6)$$

The calculated values for the *K* coefficient are provided in Table 1. In this manner, the bulk degradation mechanism can be presented by a single value, enabling easier QSA/PR modeling to establish the structural characteristics of organic pollutants that are more susceptible to HO• degradation (*K* >> 1) compared to those undergoing preferable reduction reactions via O₂•⁻ (*K* << 1).

2.2. Modeling of Degradation Mechanisms over *K* Coefficient Using QSA/PR

The methodology applied in the correlation of the calculated *K* coefficient with the structural features of 30 studied organic compounds reflected in the calculated descriptors was well established in our previous works [22,23,31]. Hence, the set of 30 organic compounds was firstly divided into training (25 compounds) and test (five compounds) sets (Table 1). QSA/PR modeling was then applied on the training set in a step-wise fashion. Hence, models with one, two, three, four, and eventually five variables (i.e., descriptors) were developed, aiming at the highest possible accuracy (based on *R*² value), simultaneously maintaining the linearity of computed models by employed QUIK rule; descriptors involved in a model cannot possess *R*_{ij} ≥ 0.6, otherwise, model is discarded. It should be noted that models with more than five variables were not considered due to the “rule of

thumb", which defines that a ratio higher than 1:5 between the number of variables (i.e., descriptors) in the model vs. number of compounds in the set used for modeling (i.e., training set) is not desirable [23,32]. Due to the fact that the ratio of the maximum and minimum value of K coefficients calculated for the selected organics was very high (~158), we tested several transformation functions (e.g., square root, log, ln, power of base 10, power of base e, etc.) to improve the modeling results. Namely, such transformations yield a narrowing of the range of responses, which usually leads to the improvement of correlation results obtained by modeling actions [31,33]. Based on the highest accuracy during preliminary modeling actions with each of applied transformation for K , we selected the $\frac{1}{\sqrt{(K+1)}}$ transformation and kept it in the further modeling. The benefit of using selected transformation is two-fold: besides having the highest accuracy due to suitable narrowing of responses range, it is not possible that model would predict the K coefficient to have a negative value, which is not practical and does not have a physical meaning.

The comparison of the performance of the one-, two-, three-, four- and five-variable QSA/PR models, selected as the best for compounds in the training and then applied on the test sets, was performed taking into account the values of statistical parameters (R^2 , Q^2 , F , p , s , S_{PRESS}); the comparative values are summarized in Table S2 (Supplementary Materials).

The main selection criterion, determining the model accuracy, was correlation coefficient of regression (R), for which a comparison of the values obtained for the training and test sets is presented in Figure 3.

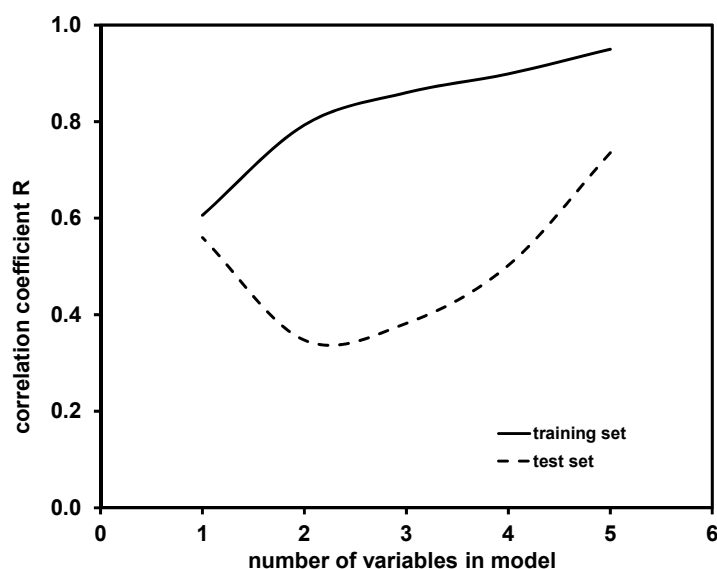


Figure 3. Comparison of correlation coefficients R obtained for training and test set by one- to five-variable models for modeling of K coefficient.

As can be observed, R values obtained for models in the training set increased with the addition of new variables into the model. A similar effect (with the exception of the one-variable model) can be observed for R values obtained for test set, yielding the highest accuracy in the case of five-variable model. It should be noted that higher-dimensional models, i.e., with more than five variables, might provide better predictability; however, such cases were not tested due to the above-mentioned *“rule of thumb”*. Hence, the five-variable model was selected as the best model among those calculated. That model was further validated using the Leave-Many-Out (LMO) technique [34] and the *“Y-scrambling”* test [35]. Graphical representations for these two validation tests are presented in Figure S1 (Supplementary Materials). It can be seen that the Q^2_{LMO} values, which are not widely scattered, are rather close to the Q^2_{LOO} value of the selected five-variable models and Q^2_{LMO} , indicating the validity of the selected QSA/PR Model (supplement, Supplementary Materials). The results of the *“Y-scrambling”* test further support the

validity of the selected five-variable model; the R^2 and Q^2_{LOO} values obtained for the five-variable model are significantly higher than the values calculated for $R^2_{\text{Y-SCRAMBLING}}$ and $Q^2_{\text{Y-SCRAMBLING}}$ (supplement, Supplementary Materials). Fitting and internal and external validation criteria values for the selected five-variable model are provided in Table S3 (Supplementary Materials).

The performance of the selected five-variable model, when applied on the entire set (i.e., all 30 organic compounds studied), is shown in Figure 4, while the model equation is presented below (7), along with the values of corresponding statistical parameters determining its accuracy and significance.

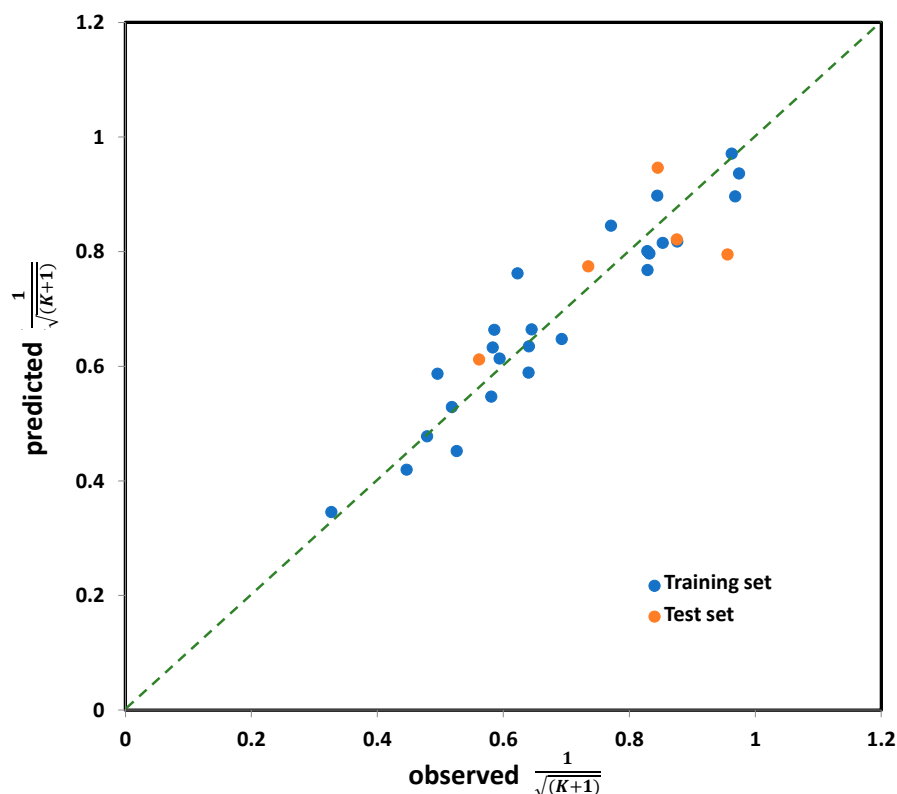


Figure 4. The observed vs. predicted values for K coefficient (in transformed $\frac{1}{\sqrt{K+1}}$ form), for the entire set (30 compounds) calculated by five-variable model, selected as the best one among all tested.

$$Y\left(\frac{1}{\sqrt{K+1}}\right) = -0.327 (\pm 0.086) \times \text{MATS4v} - 0.245 (\pm 0.086) \times \text{Mor10u} \\ + 0.165 (\pm 0.061) \times \text{CATS2D_01_DN} - 0.176 (\pm 0.076) \times \text{B04[C - Cl]} \\ + 0.151 (\pm 0.067) \times \text{B08[C - O]} + 0.533 (\pm 0.053) \quad (7)$$

$$(n = 30; R^2 = 0.876; s = 0.069; F = 33.665; p < 0.0001; Q^2 = 0.816; S_{\text{PRESS}} = 0.084; S_{\text{DEP}} = 0.076)$$

Based on the descriptive statistical data of the coefficients included in Model (7) that are summarized in Table S4 (Supplementary Materials), it can be concluded that all model terms are significant (i.e., all possess $p_T < 0.05$). The correlation matrix confirming model linearity (descriptor pairs has $R_{ij} < 0.6$) is provided in Table S5 (Supplementary Materials). As can be observed from Figure 4, the points or point clusters are placed rather close to the regression diagonal line, indicating on the high accuracy of selected five-variable Model (7). The applicability domain test of selected five-variable model was assessed employing a Williams plot (Figure 5). Leveraging such an approach enables detection of both highly structurally influential chemicals and response outliers. Hence, the limit on the x axis (h_{ii}), which is calculated as $h_{ii} = 3(m + 1)/n$, where m and n stands for number of variables in the model and number of compounds in the training set, respectively, determines the structurally influential chemicals (based on HAT values). The limits on the y axis are set at $\pm 3.0\sigma$, and determine the response outliers (based on standardized RES values); these can

also be associated with potential experimental errors [36]. As can be observed from Figure 5, there are no response outliers, which speaks in favor of high model predictivity, validity and accuracy. Based on the fact that there are no structurally influenced compounds (i.e., X outliers), it can be concluded that model is robust regarding the diversity of molecular structures of organic compounds.

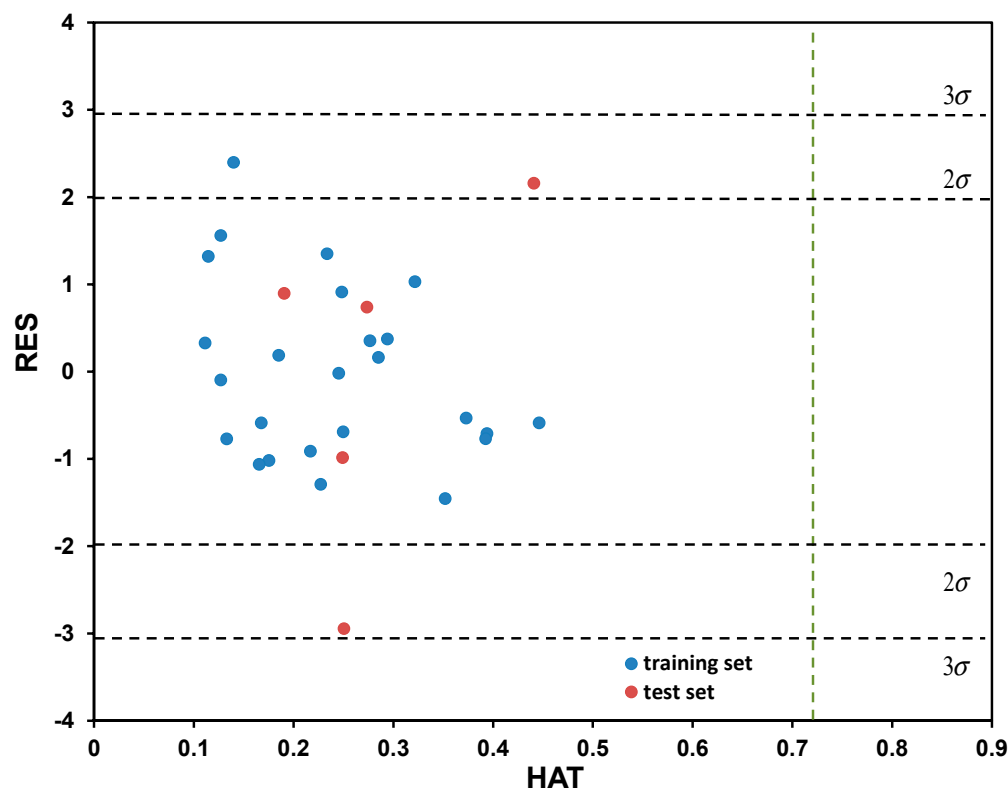


Figure 5. Determination of applicability domain (AD) for the five-variable model, selected as the best among tested, through Williams plot.

The names, short descriptions and pertaining classes of descriptors included in the five-variable Model (7) are provided in Table 2. As can be observed, the included descriptors belong to following classes: 2D autocorrelations, 3D-MoRSE, CATS2D and 2D Atom Pairs. The first three mentioned classes include descriptors calculated by rather complex schemes, while the latter represent the occurrence of exact atom pairs at certain topological distances in the molecules. Descriptors pertaining to 2D-autocorrelations are calculated based on molecular graphs and specific algorithms such as the Broto-Moreau (AST), Geary (GATS) and Moran (MATS). Accordingly, the descriptors are denoted by the algorithm abbreviation, along with numerical properties assigned to atoms (the so-called “lag”) and the abbreviation of specific weighting scheme (*m* (relative atomic mass), *p* (polarizability), *e* (Sanderson electronegativity), *v* (Van der Waals volume), *i* (ionization potential) and *s* (I-state; electrotopological states)) [37]. Descriptors pertaining to 3D-MoRSE class (3D Molecule Representation of Structures based on Electron diffraction) are calculated by summing atom weights viewed by different angular scattering function and are denoted with the abbreviation Mor, the number for the signal, ranging from 1 to 32, and the abbreviation of the specific weighting scheme (*m*, *p*, *e*, *v*, *i* and *s*) [37]. The CATS2D class includes topological pharmacophore descriptors that are based on auto- and cross-correlation of five different pharmacophoric atom types: H-bond donor (D), H-bond acceptor (A), positively charged (P), negatively charged (N), and lipophilic (L) [38,39]. Hence, any atom in the molecule can be assigned to none, one, or two of the mentioned types, yielding 15 combinations for atom pairs. Since CATS2D descriptors are computed with the topological distance (i.e., lag) ranging from 0 to 9, overall, 150 frequencies are possible.

Table 2. Definitions of descriptors included in the five-variable model for prediction of *K* coefficient.

Descriptor Name	Descriptor Definition	Descriptor Type
MATS4v	Moran autocorrelation of lag 4 weighted by van der Waals volume	2D autocorrelations
Mor10u	signal 10/unweighted	3D-MoRSE
CATS2D_01_DN	CATS2D Donor-Negative at lag 01	CATS 2D
B04[C – Cl]	Presence/absence of C – Cl at topological distance 4	2D Atom Pairs
B08[C – O]	Presence/absence of C O at topological distance 8	2D Atom Pairs

2.3. Structural Features Determining Photocatalytic Degradation Mechanisms Occurring in the Bulk

Taking into account the values of indexes of descriptors included in Model (7), the contribution of molecular features preferring degradation via HO• or O₂•[−] can be established. The highest contribution to the response was showed by **MATS4v**, and due to the negative index of its coefficient, this contribution is antagonistic. However, it should be noted that we used the transformed value of *K* coefficient in a form $\frac{1}{\sqrt{(K+1)}}$; thus, the lower the value of transformed *K*, the higher the original *K* value. Accordingly, what has an antagonistic effect on transformed *K* will have a synergistic effect on original *K*, meaning that the higher the *K* coefficient, the higher the portion of organic compound degraded by HO• and vice versa for O₂•[−]. The other four included descriptors have lower absolute values of coefficients: approximately 25% (**Mor10u**), 46% (**B04[C – Cl]**), 50% (**CATS2D_01_DN**) and 54% (**B08[C – O]**). **Mor10u** and **B04[C – Cl]** have negative indexes of coefficients, having antagonistic effects on transformed *K*, but synergistic on original *K* values (i.e., denoting structural features that promote degradation via HO•). On the other hand, indexes of **CATS2D_01_DN** and **B08[C – O]** coefficients are positive, contributing eventually negatively to original *K* values (i.e., denoting structural characteristics more susceptible to degradation via reductive reaction by O₂•[−]). Although several descriptors were obtained using the rather complex calculations, their weighting schemes may indicate the structural features more clearly. However, the descriptor **Mor10u** is unweighted. On the other hand, *v*, as the weighting scheme in the 2D-autocorrelation descriptor **MATS4v**, indicates the importance of Van der Waals volume, also called molecular volume and denoting the volume “occupied” by a molecule, as a general structural characteristic of a molecule attacked more preferably by either HO• or O₂•[−]. Thus, it can be concluded that the size matters. The other three included descriptors provide more straightforward correlation of particular structural characteristics promoting the HO• driven degradation over that by O₂•[−]. Hence, **CATS2D_01_DN** denotes a preferred topological distance (one bond) between H-bond donor and negative centers. This descriptor is characteristic for several compounds in the studied set of organics and amounts to either 1 (possessing this descriptor; compounds possessing carboxylic group (-COOH)) or 0 (compounds without this feature). Since **CATS2D_01_DN** has a positive index in Model (2), negatively contributing to the *K* value, compounds with carboxylic group are preferably degraded by O₂•[−]. Although Chen et al. [19] emphasized the importance of carboxylic group moiety in photocatalytic degradation, a deeper correlation with the occurring mechanism and undergoing pathway was not provided. Actually, they assumed that this moiety was important within the adsorption step, which would then lead to direct degradation at the catalyst surface. However, it should be emphasized that we investigated only the indirect degradation mechanism occurring in the bulk. Furthermore, Xiao et al. [40] clearly demonstrated the role of reductive ROS in the degradation of -COOH-containing compounds; when the UV/Ag-TiO₂ system was purged by N₂, which diminished the dissolved O₂ and consequently the formation of O₂•[−], their degradation was greatly inhibited. Hence, our results, obtained with a set of chemicals with more diversified structural differences, clearly revealed that this moiety would be favorably degraded by reduction reactions, supporting findings presented in [40]. The same influence on *K* is possessed by **B08[C – O]**, which corresponds to the presence/absence of the C–O bond at a topological distance of 8. This structural feature is

characteristic for most of the CECs in the studied set, while smaller single-benzene-ring compounds are discarded due to the maximal number of C atoms either in molecule in general or C atom at too far distance from O atom. Hence, compounds possessing O as a heteroatom, either in $-\text{COOH}$, $-\text{O}-$, or $-\text{OH}$ moieties, at this topological distance from the C atom represent preferable structural features promoting reductive degradation via $\text{O}_2\bullet^-$. As Model (7) possesses a negative index, the descriptor **B04[C – Cl]**, which denotes the presence/absence of the C–Cl bond at a topological distance of 4, represents a structural feature preferring $\text{HO}\bullet$ oxidative degradation over reduction via $\text{O}_2\bullet^-$. It should be noted that this structural feature is correlated with most of the studied organics that possess Cl as a heteroatom. The exception is AZN; although it possesses Cl, it is not counted within the **B04[C – Cl]** descriptor because the topological distance between the C and Cl atoms is lower than 4. The importance of this structural feature for favoring $\text{HO}\bullet$ reactions can be correlated with known degradation pathways upon attack by $\text{HO}\bullet$. Namely, there are three main pathways: (i) H-abstraction (which is followed by subsequent hydroxylation); (ii) single electron transfer (SEC); and (iii) radical addition (RA) [21]. It has been established that H-abstraction is the most preferable pathway [23,26]. Hence, in a case when halide atom (e.g., Cl) is bonded to the aromatic ring, the H-abstraction pathway would comprehend the breaking of the next C–H, followed by hydroxylation at the same position in the structure. This sequence would be repeated up until ring saturation, which is then followed by its cleavage and consequently formation of open-ring, aliphatic by-products. This action is preferable to Cl atom release due to reduction reaction, which is actually mediated by $\text{O}_2\bullet^-$ [41–43].

3. Materials and Methods

3.1. Chemicals

The 30 selected compounds, including 19 CECs (pharmaceuticals, pesticides, and plasticizers) and 11 common single-benzene ring aromatics, along with their names, abbreviations, CAS number, and molecular formulas, are provided in Table 1, while their structures are presented in Figure S2 (Supplementary Materials). As mentioned, the studied set includes, besides CECs, single-benzene-ring aromatics that are often used as coupling compounds for CECs or are determined as their degradation by-products. Table 1 also summarizes the calculated values of K coefficient (in both original and transformed values), which presents the ratio of their degradation extents in a bulk phase by $\text{HO}\bullet$ and $\text{O}_2\bullet^-$; $M_{\text{HO}\bullet}/M_{\text{O}_2\bullet^-}$. All studied organics were purchased from either Sigma Aldrich, Saint Louis, MO, or Acros Chemicals, New Jersey, NJ (both USA). The following chemicals were also used in the study either as (i) constituents of mobile phases in HPLC analysis (formic acid (HPLC grade, Sigma Aldrich, Saint Louis, MO, USA), oxalic acid (p.a., Sigma Aldrich, Saint Louis, MO, USA), methanol and acetonitrile (both HPLC grade, J.T. Baker, Phillipsburg, NJ, USA)); (ii) scavengers for $\text{HO}\bullet$ and $\text{O}_2\bullet^-$ mediated bulk reactions (dimethyl sulfoxide ($(\text{CH}_3)_2\text{SO}$, DMSO, 99.9%, Sigma Aldrich, Saint Louis, MO, USA), and 1,4-benzoquinone ($\text{C}_6\text{H}_4\text{O}_2$, BQ, 98%, Fluka, Buchs, Switzerland), respectively); or (iii) for pH adjustments (sulfuric acid (H_2SO_4) and sodium hydroxide (NaOH) (both p.a., Kemika, Zagreb, Croatia)). All aqueous solutions were prepared using MilliQ-water, obtained by Direct-Q3 UV (Merck Millipore, Darmstadt, Germany) ultrapure water system. The most commonly studied photocatalytic material, Aeroxide TiO_2 P25 (Evonik, Essen, Germany), was used for UVA-driven treatment of studied organics in the presence and absence of above-mentioned ROS scavengers (DMSO and BQ).

3.2. Experimental Procedure

Model solutions of selected organic compounds (Table 1) with initial concentration of 0.05 mM were treated in a borosilicate-glass cylinder batch photoreactor ($V = 0.08$ L) with water-jacket cooling, ensuring constant temperature of reaction solution ($T = 25.0 \pm 0.2$ °C). A light source (Pen-ray, UVP, Cambridge, UK) emitting monochromatic irradiation at 365 nm ($P_0 = 96$ $\mu\text{W}/\text{cm}^2$) was placed vertically in the middle of the reactor ($L = 1$ cm) in

the quartz cuvette. The reactor was equipped with the magnetic stirrer to provide effective mixing of the reaction solution. The experiments were conducted respecting following procedure: (i) model solutions of selected organics were placed into the reactor; (ii) the appropriate amount of TiO_2 P25 photocatalyst was added (0.8 g L^{-1}); and (iii) pH was adjusted to 7 using H_2SO_4 or NaOH . (iv) The solution was then stirred in a dark for 30 min (based on the preliminary tests) to establish adsorption equilibrium; and (v) afterwards, the warmed-up UVA lamp was inserted in quartz cuvette and the treatment started. For each of the selected organics, three types of photocatalytic experiments were performed: (i) without scavenging agents; (ii) with DMSO (10 mM); and (iii) with BQ (10 mM) presence to suppress bulk degradation mediated by $\text{HO}\bullet$ and $\text{O}_2\bullet^-$, respectively. The duration of experiments was 50 min (30 min dark period and 20 min under UVA illumination). During the experiments, 500 μL aliquots were periodically taken at -20 , -10 (during dark period), 0 (starting of irradiation), 2.5, 5, 10, 15, and 20 min, filtered using Chromafil XTRA RC (25 mm, $0.45 \mu\text{m}$, Macherey Nagel, Duren, Germany), quenched with MeOH and submitted to HPLC analysis. The experiments were conducted in quintuplicates and average values were reported; the reproducibility of experiments calculated based on HPLC measurements was 97.3%.

3.3. Analytical Procedure

Changes in the concentration of studied organic compounds in aqueous phase were monitored by high-performance liquid chromatography (HPLC, LC20, Shimadzu, Kyoto, Japan) equipped with UV-DAD detector (SPD-M20A, Shimadzu, Japan), two pumps and degassing unit. The injection volume was 50 μL with mobile phase flow set at 0.5 mL min^{-1} . The composition of mobile phase and columns applied for the detection varied depending on the organic compound analyzed; details of HPLC analysis (including detection wavelengths) are summarized in Table S6 (Supplementary Materials). A Handylab pH/LF portable pH meter (Schott Instruments GmbH, Mainz, Germany) was used for pH adjustment monitoring.

3.4. Computational Part

The set of 30 organic compounds (along with calculated values of K coefficient) was divided into a training set (25 compounds) and a test set (5 compounds) (Table 1), respecting the same intervals of chosen responses and that extreme values are present only in a training set.

Molecular structures of organic compounds studied were built using GaussView 6.0 software (Gaussian, Inc., Wallingford, USA). The built molecular structures were then optimized using chemical density functional theory (DFT) methods (B3LYP/6-311++G(d,p)), employing Gaussian16 (Gaussian Inc., Wallingford, CT, USA) [44,45]. During this modeling action, several empirical quantum chemical parameters—(i) dipole moment (total μ , as well as its X, Y, and Z components), (ii) energy of the highest (E_{HOMO}) and (iii) the lowest occupied molecular orbital (E_{LUMO}) and (iv) the gap between (HLG), (v) final heat of formation (ΔH_f), and (vi) ionization potential—were calculated and later used as theoretical descriptors. The majority of the molecular descriptors were calculated employing DRAGON 6.0 software (Milano Chemometrics and QSAR Research Group, TALETE, Milano, Italy) using optimized molecular structures of studied organic compounds by DFT. In this manner, 3129 molecular descriptors were obtained which captured relevant structural features of studied organic compounds, thus describing their chemical diversities.

The correlation between QSA/PR responses (K coefficients) and descriptors calculated by DRAGON and DFT was obtained employing the combined approach which included variable selection Genetic Algorithm (GA) and Multiple Linear Regression Analysis (MLRA) embedded within QSARINS 2.2.4 (QSAR Group, University of Insubria, Italy) [46–48]. In this manner, the most influential descriptors were selected within built 1–5-variable models (i.e., including 1 to 5 descriptors). The GA variable selection technique started with

following parameters: 200 random models, the generation size of 2000 iterations, and the mutation probability specified as 20%.

Before the above-mentioned modeling actions using QSARINS 2.2.4 software, the descriptor matrix was screened for highly intercorrelated and redundant descriptors. Accordingly, descriptor pairs with R values ≥ 0.99 were removed (overall, 496 descriptors). In this manner, the overall number of descriptors in the matrix was reduced to 2642, including 2633 Dragon calculated and 9 computed by DFT. In order to enable the comparison of contributions of descriptors involved in generated QSA/PR models to the end-point responses (i.e., K coefficients), descriptor matrix was then normalized. During GA and MLRA modeling actions, the filtering rules were employed to discard models with either highly correlated descriptors ($R_{ij} > 0.6$) or those with the inadequate significance (p_M or $p_T \geq 0.05$); QUIK rule was applied prior modeling, CI rule was activated after models were built. The validation and verification of models was based on common statistical parameters (Table 3), as well as Leave Many Out (LMO) and “Y-scrambling” tests. The applicability domain (AD) of the selected models was estimated using a Williams plot [49], where the response outliers and structurally influential compounds could be straightforwardly detected.

Table 3. Definitions of descriptors included in five-variable model for the prediction of the K coefficient.

#	Symbol	Definition
1	R	the correlation coefficient of regression
2	R^2	the model explained variance
3	Q^2	the leave-one-out cross-validation coefficient
4	F	F-ratio between variances of observed and calculated values
5	p	probability value for calculated F
6	s	standard error
7	S_{PRESS}	standard error of the predictive residue of sum of squares

4. Conclusions

A QSA/PR model was developed aiming at describing the structural diversity of contaminants of emerging concern (CECs) during photocatalytic treatment susceptible to the occurrence of oxidative and reductive mechanisms driven by $\text{HO}\bullet$ and $\text{O}_2\bullet^-$, respectively. First, we determined the degradation rates of the targeted organics in the absence and presence of common scavengers for $\text{HO}\bullet$ and $\text{O}_2\bullet^-$ during their photocatalytic treatment. The obtained values were then brought into correlation via the K coefficient, denoting the ratio of organics degraded by two occurring mechanisms; $K \gg 1$ compounds are more susceptible to $\text{HO}\bullet$ degradation, while $K \ll 1$ compounds prefer reduction reactions driven by $\text{O}_2\bullet^-$. The values of K coefficient were then used as responses in quantitative structure–property relationship (QSA/PR) modeling. The QSA/PR modeling included validation over internal validation parameters, as well as by Leave-Many-Out (LMO) and “Y-scrambling” tests, which showed that the selected model was statistically significant. Furthermore, the applicability domain of the model selected as the best was defined by the leverage approach using a Williams plot to detect the highly structurally influential chemicals and response outliers.

The results of the QSA/PR modeling revealed that structural features such as the size of the molecules, represented by the MATS4v descriptor, influence the degradation rate in general. Furthermore, the presence/absence of particular molecular fragments such as C – O (particularly in a form of carboxyl group), represented by CATS2D_01_DN and B08[C – O] descriptors, and C – Cl bonds, represented by the B04[C – Cl] descriptor, dictate the preferable degradation pathway of CECs by photocatalytic degradation; the latter favors $\text{HO}\bullet$ driven reaction, while the former favors the reductive pathway. The developed QSA/PR models can be considered robust predictive tools for evaluating distribution between degradation mechanisms occurring in photocatalytic treatment, and

guidance for tailoring photocatalyst to favor oxidative or reductive reactions, depending on the structure of targeting pollutants.

Supplementary Materials: The following supporting information can be downloaded at: <https://www.mdpi.com/article/10.3390/molecules28062443/s1>, Figure S1: Scatter plots of LMO and Y-scrambling model compared to the 5-variable QSA/PR model; Figure S2: Molecular structures of studied contaminants of emerging concern and single-benzene ring compounds; Table S1: Experimental results on the removal and degradation of studied organics by UVA/TiO₂ process (pH₀ 7 and TiO₂ loading of 0.8 gL⁻¹); Table S2: Statistical evaluation of QSA/PR models for training set (25 compounds) and test set (5 compounds); Table S3: Values of fitting, internal and external validation criteria of selected best 5-variable model; Table S4: Descriptive statistical data included in the best 5-variable model; Table S5: Correlation matrix of descriptors included in best 5 variable model for entire set of compounds (cross-correlation $R_{ij} < 0.6$); Table S6: Composition of mobile phases and detection details for HPLC analysis of 30 studied organics.

Author Contributions: Conceptualization, H.K. and A.L.B.; formal analysis, A.T., M.K., P.K. and B.R.; investigation, A.T. and M.K.; data curation, A.T., M.K., H.K., P.K. and B.R.; writing—original draft preparation, A.T., M.K. and H.K.; writing—review and editing, H.K., P.K., B.R. and A.L.B.; funding acquisition, H.K. All authors have read and agreed to the published version of the manuscript.

Funding: This research was funded by Croatian Science Foundation (Nano-sized Solar-active Catalysts for Environmental Technologies, NaSCeNT, IP-2018-01-1982) and Croatian Government and the European Union through the European Regional Development Fund (Water Purification and Energy Conversion using Novel Composite Materials and Solar Irradiation, KK.01.1.1.04.0001). This work was also supported in part by the National Science Foundation (NSF) MRI award OAC-2019077.

Institutional Review Board Statement: Not applicable.

Informed Consent Statement: Not applicable.

Data Availability Statement: The datasets collected and analyzed within this work are available from the corresponding authors upon written request.

Acknowledgments: The authors would like to thank the Extreme Science and Engineering Discovery Environment (XSEDE) for the award allocation (TG-DMR110088). We also gratefully acknowledge Paola Gramatica for enabling a free license of software QSARins (version 2.2.4).

Conflicts of Interest: The authors declare no conflict of interest.

Sample Availability: Samples of the compounds are not available from the authors.

References

1. Golovko, O.; Örn, S.; Söregård, M.; Frieberg, K.; Nassazzi, W.; Lai, F.Y.; Ahrens, L. Occurrence and removal of chemicals of emerging concern in wastewater treatment plants and their impact on receiving water systems. *Sci. Total Environ.* **2021**, *754*, 142122. [[CrossRef](#)] [[PubMed](#)]
2. Meyer, M.F.; Powers, S.M.; Hampton, S.E. An Evidence Synthesis of Pharmaceuticals and Personal Care Products (PPCPs) in the Environment: Imbalances among Compounds, Sewage Treatment Techniques, and Ecosystem Types. *Environ. Sci. Technol.* **2019**, *53*, 12961–12973. [[CrossRef](#)]
3. Söregård, M.; Campos-Pereira, H.; Ullberg, M.; Lai, F.Y.; Golovko, O.; Ahrens, L. Mass loads, source apportionment, and risk estimation of organic micropollutants from hospital and municipal wastewater in recipient catchments. *Chemosphere* **2019**, *234*, 931–941. [[CrossRef](#)] [[PubMed](#)]
4. Gago-Ferrero, P.; Gros, M.; Ahrens, L.; Wiberg, K. Impact of on-site, small and large scale wastewater treatment facilities on levels and fate of pharmaceuticals, personal care products, artificial sweeteners, pesticides, and perfluoroalkyl substances in recipient waters. *Sci. Total Environ.* **2017**, *601–602*, 1289–1297. [[CrossRef](#)]
5. Patel, M.; Kumar, R.; Kishor, K.; Mlsna, T.; Pittman, C.U.; Mohan, D. Pharmaceuticals of emerging concern in aquatic systems: Chemistry, occurrence, effects, and removal methods. *Chem. Rev.* **2019**, *119*, 3510–3673. [[CrossRef](#)] [[PubMed](#)]
6. Rath, B.S.; Kumar, P.S.; Show, P.L. A review on effective removal of emerging contaminants from aquatic systems: Current trends and scope for further research. *J. Hazard. Mater.* **2021**, *409*, 124413. [[CrossRef](#)]
7. Coimbra, R.N.; Escapa, C.; Otero, M. Removal of pharmaceuticals from water: Conventional and alternative treatments. *Water Switz.* **2021**, *13*, 487. [[CrossRef](#)]
8. Kanakaraju, D.; Glass, B.D.; Oelgemöller, M. Advanced oxidation process-mediated removal of pharmaceuticals from water: A review. *J. Environ. Manag.* **2018**, *219*, 189–207. [[CrossRef](#)]

9. Kovacic, M.; Kusic, H.; Loncaric Bozic, A.; Dionysiou, D.D. Advanced Oxidation Processes. In *Encyclopedia of Water: Science, Technology, and Society*; Wiley: Hoboken, NJ, USA, 2020; pp. 1925–1940.
10. Chen, D.; Cheng, Y.; Zhou, N.; Chen, P.; Wang, Y.; Li, K.; Huo, S.; Cheng, P.; Peng, P.; Zhang, R.; et al. Photocatalytic degradation of organic pollutants using TiO₂-based photocatalysts: A review. *J. Clean. Prod.* **2020**, *268*, 121725. [[CrossRef](#)]
11. Lee, C.M.; Palaniandy, P.; Dahlan, I. Pharmaceutical residues in aquatic environment and water remediation by TiO₂ heterogeneous photocatalysis: A review. *Environ. Earth Sci.* **2017**, *76*, 611. [[CrossRef](#)]
12. Snowdon, M.; Liang, R.; Van Leeuwen, J.C.; Schneider, O.; Khan, A.; Li, L.C.M.; Fong, C.; Zhou, N.Y.; Servos, M.R. Pharmaceutical Micropollutant Treatment with UV-LED/TiO₂ Photocatalysis under Various Lighting and Matrix Conditions. *Photochem* **2022**, *2*, 503–514. [[CrossRef](#)]
13. Andronic, L.; Isac, L.; Miralles-Cuevas, S.; Visa, M.; Oller, I.; Duta, A.; Malato, S. Pilot-plant evaluation of TiO₂ and TiO₂-based hybrid photocatalysts for solar treatment of polluted water. *J. Hazard. Mater.* **2016**, *320*, 469–478. [[CrossRef](#)]
14. Luna-Sanguino, G.; Ruíz-Delgado, A.; Tolosana-Moranchel, A.; Pascual, L.; Malato, S.; Bahamonde, A.; Faraldos, M. Solar photocatalytic degradation of pesticides over TiO₂-rGO nanocomposites at pilot plant scale. *Sci. Total Environ.* **2020**, *737*, 140286. [[CrossRef](#)] [[PubMed](#)]
15. Pichat, P. *Photocatalysis and Water Purification*; Wiley-VCH: Weinheim, Germany, 2013.
16. dela Rosa, F.; Popović, M.; Papac Zjačić, J.; Radić, G.; Kraljić Roković, M.; Kovačić, M.; José Farré, M.; Genorio, B.; Lavrenčić Štangar, U.; Kušić, H.; et al. A Visible light activation of persulfate or H₂O₂ by TiO₂/Fe₂O₃ immobilized on glass support for photocatalytic removal of amoxicillin: Mechanism, transformation products and toxicity assessment. *Nanomaterials* **2022**, *12*, 4328. [[CrossRef](#)]
17. Matoh, L.; Zener, B.; Kovacic, M.; Kusic, H.; Arcon, I.; Levstek, M.; Lavrencic Stangar, U. Photocatalytic sol-gel/P25 TiO₂ coatings for water treatment: Degradation of 7 selected pharmaceuticals. *Ceram. Inter.* **2022**, *in press*. [[CrossRef](#)]
18. Sruthi, L.; Janani, B.; Sudheer Khan, S. Ibuprofen removal from aqueous solution via light-harvesting photocatalysis by nano-heterojunctions: A review. *Sep. Pur. Technol.* **2021**, *27915*, 119709. [[CrossRef](#)]
19. Chen, Q.; Song, J.M.; Pan, F.; Xia, F.L.; Yuan, J.Y. The kinetics of photocatalytic degradation of aliphatic carboxylic acids in an UV/TiO₂ suspension system. *Environ. Technol.* **2009**, *30*, 1103–1109. [[CrossRef](#)]
20. Yin, R.; Ling, L.; Lu, S.; Li, H.; Li, C.; Shang, C. Degradation of aliphatic halogenated contaminants in water by UVA/Cu-TiO₂ and UVA/TiO₂ photocatalytic processes: Structure-activity relationship and role of reactive species. *Chemosphere* **2020**, *260*, 127644. [[CrossRef](#)]
21. Huang, X.; Feng, Y.; Hu, C.; Xiao, X.; Yu, D.; Zou, D. Mechanistic QSAR models for interpreting degradation rates of sulfonamides in UV-photocatalysis systems. *Chemosphere* **2015**, *138*, 183–189. [[CrossRef](#)]
22. Kušić, H.; Rasulev, B.; Leszczynska, D.; Leszczynski, J.; Koprivanac, N. Prediction of rate constants for radical degradation of aromatic pollutants in water matrix: A QSAR study. *Chemosphere* **2009**, *75*, 1128–1134. [[CrossRef](#)]
23. Cvetnić, M.; Kovacic, M.; Novak Stankov, M.; Ukić, Š.; Bolanča, T.; Kušić, H.; Rasulev, B.; Dionysiou, D.D.; Lončarić Božić, A. Key structural features promoting radical driven degradation of emerging contaminants in water. *Environ. Inter.* **2019**, *124*, 38–48. [[CrossRef](#)] [[PubMed](#)]
24. Güsten, H. Predicting the abiotic degradability of organic pollutants in the troposphere. *Chemosphere* **1999**, *38*, 1361–1370. [[CrossRef](#)]
25. Gramatica, P.; Pilutti, P.; Papa, E. A tool for the assessment of VOC degradability by tropospheric oxidants starting from chemical structure. *Atmos. Environ.* **2004**, *38*, 6167–6175. [[CrossRef](#)]
26. Luo, X.; Yang, X.; Qiao, X.; Wang, Y.; Chen, J.; Wei, X.; Peijnenburg, W.J.G.M. Development of a QSAR model for predicting aqueous reaction rate constants of organic chemicals with hydroxyl radicals. *Environ. Sci. Process. Impacts* **2017**, *19*, 350–356. [[CrossRef](#)] [[PubMed](#)]
27. Ren, M.; Sun, S.; Wu, Y.; Shi, Y.; Wang, Z.-J.; Cao, H.; Xie, Y. The structure-activity relationship of aromatic compounds in advanced oxidation processes: A review. *Chemosphere* **2022**, *296*, 134071. [[CrossRef](#)]
28. Sharifi, T.; Crmaric, D.; Kovacic, M.; Popovic, M.; Rokovic, M.K.; Kusic, H.; Jozić, D.; Ambrožić, G.; Kralj, D.; Kontrec, J.; et al. Tailored BiVO₄ for enhanced visible-light photocatalytic performance. *J. Environ. Chem. Eng.* **2021**, *9*, 106025. [[CrossRef](#)]
29. Buxton, G.V.; Greenstock, C.L.; Helman, W.P.; Ross, A.B. Critical review of rate constants for reactions of hydrated electrons, hydrogen atoms and hydroxyl radicals (•OH/•O⁻) in aqueous solution. *J. Phys. Chem. Ref. Data* **1988**, *17*, 513–586. [[CrossRef](#)]
30. Fónagy, O.; Szabó-Bárdos, E.; Horváth, O. 1,4-Benzoquinone and 1,4-hydroquinone based determination of electron and superoxide radical formed in heterogeneous photocatalytic systems. *J. Photochem. Photobiol. A Chem.* **2021**, *407*, 113057. [[CrossRef](#)]
31. Tomic, A.; Cvetnic, M.; Kovacic, M.; Kusic, H.; Karamanis, P.; Loncaric, A. Structural features promoting adsorption of contaminants of emerging concern onto TiO₂ P25: Experimental and computational approaches. *Environ. Sci. Pollut. Res.* **2022**, *28*, 1–17. [[CrossRef](#)]
32. Gramatica, P. Chemometric Methods and Theoretical Molecular Descriptors in Predictive QSAR Modeling of the Environmental Behavior of Organic Pollutants. In *Recent Advances in QSAR Studies*; Springer: Berlin/Heidelberg, Germany, 2010.
33. Smidt, M.; Kusic, H.; Juretic, D.; Stankov, M.N.; Ukić, S.; Bolanca, T.; Rogosic, M.; Bozic, A.L. Modeling Photo-oxidative Degradation of Aromatics in Water. Optimization Study Using Response Surface and Structural Relationship Approaches. *Ind. Eng. Chem. Res.* **2015**, *54*, 5427–5441. [[CrossRef](#)]
34. Wehrens, R.; Putter, H.; Buydens, L.M.C. The bootstrap: A tutorial. *Chemom. Intell. Lab. Syst.* **2000**, *54*, 35–52. [[CrossRef](#)]

35. Rücker, C.; Rücker, G.; Meringer, M. Y-randomization and its variants in QSPR/QSAR. *J. Chem. Inf. Model.* **2007**, *47*, 2345–2357. [[CrossRef](#)] [[PubMed](#)]
36. Liu, H.; Papa, E.; Gramatica, P. Evaluation and QSAR modeling on multiple endpoints of estrogen activity based on different bioassays. *Chemosphere* **2008**, *70*, 1889–1897. [[CrossRef](#)] [[PubMed](#)]
37. Todeschini, R.; Consonni, V. Handbook of Molecular Descriptors. In *Handbook of Chemoinformatics: From Data to Knowledge*; Gasteiger, J., Ed.; Wiley-VCH Verlag GmbH: Weinheim, Germany, 2003.
38. Dreher, J.; Scheiber, J.; Stiefl, N.; Baumann, K. XMaP—An Interpretable Alignment-Free Four-Dimensional Quantitative Structure-Activity Relationship Technique Based on Molecular Surface Properties and Conformer Ensembles. *J. Chem. Inf. Model.* **2018**, *58*, 165–181. [[CrossRef](#)] [[PubMed](#)]
39. Leszczynski, J.; Kaczmarek-Kedziera, A.; Puzyn, T.; Papadopoulos, M.G.; Reis, H.; Shukla, M.K. *Handbook of Computational Chemistry*; Springer: Berlin/Heidelberg, Germany, 2017.
40. Xiao, J.; Xie, Y.; Han, Q.; Cao, H.; Wang, Y.; Nawaz, F.; Duan, F. Superoxide radical-mediated photocatalytic oxidation of phenolic compounds over Ag⁺/TiO₂: Influence of electron donating and withdrawing substituents. *J. Hazard Mater.* **2016**, *304*, 126–133. [[CrossRef](#)]
41. Kralik, P.; Kusic, H.; Koprivanac, N.; Loncaric Bozic, A. Degradation of chlorinated hydrocarbons by UV/H₂O₂: The application of experimental design and kinetic modeling approach. *Chem. Eng. J.* **2010**, *158*, 154–166. [[CrossRef](#)]
42. Lai, F.; Tian, F.X.; Xu, B.; Ye, W.K.; Gao, Y.Q.; Chen, C.; Xing, H.B.; Wang, B.; Xie, M.J.; Hu, X.J. A comparative study on the degradation of phenylurea herbicides by UV/persulfate process: Kinetics, mechanisms, energy demand and toxicity evaluation associated with DBPs. *Chem. Eng. J.* **2022**, *428*, 132088. [[CrossRef](#)]
43. Zhang, Y.; Xiao, Y.; Zhang, Y.; Lim, T.T. UV direct photolysis of halogenated disinfection byproducts: Experimental study and QSAR modeling. *Chemosphere* **2019**, *235*, 719–725. [[CrossRef](#)] [[PubMed](#)]
44. Belelli, P.G.; Ferullo, R.M.; Branda, M.M.; Castellani, N.J. Theoretical modeling of photocatalytic active species on illuminated TiO₂. *Appl. Surf. Sci.* **2007**, *254*, 32–35. [[CrossRef](#)]
45. Wang, Y.; Tang, W.; Peng, Y.; Chen, Z.; Chen, J.; Xiao, Z.; Zhao, X.; Qu, Y.; Li, J. Predicting the adsorption of organic pollutants on boron nitride nanosheets: Via in silico techniques: DFT computations and QSAR modeling. *Environ. Sci. Nano.* **2021**, *8*, 795–805. [[CrossRef](#)]
46. Gramatica, P. Principles of QSAR Modeling: Comments and Suggestions from Personal Experience. *Int. J. Quant. Struct. Relationships* **2020**, *5*, 61–97. [[CrossRef](#)]
47. Gramatica, P.; Cassani, S.; Chirico, N. QSARINS-Chem: Insubria datasets and new QSAR/QSPR models for environmental pollutants in QSARINS. *J. Comput. Chem.* **2014**, *35*, 1036–1044. [[CrossRef](#)] [[PubMed](#)]
48. Gramatica, P.; Chirico, N.; Papa, E.; Cassani, S.; Kovarich, S. QSARINS: A new software for the development, analysis, and validation of QSAR MLR models. *J. Comput. Chem.* **2013**, *34*, 2121–2132. [[CrossRef](#)]
49. Gramatica, P. Principles of QSAR models validation: Internal and external. *QSAR Comb. Sci.* **2007**, *26*, 694–701. [[CrossRef](#)]

Disclaimer/Publisher's Note: The statements, opinions and data contained in all publications are solely those of the individual author(s) and contributor(s) and not of MDPI and/or the editor(s). MDPI and/or the editor(s) disclaim responsibility for any injury to people or property resulting from any ideas, methods, instructions or products referred to in the content.